IOP Publishing Journal of Physics: Condensed Matter
J. Phys.: Condens. Matter **32** (2020) 145302 (15pp) https://doi.org/10.1088/1361-648X/ab601a

Influence of surfactant, particle size and dispersion medium on surface plasmon resonance of silver nanoparticles

Vikash Sharma[1], **Divya Verma**[2] **and Gunadhor Singh Okram**[1]

[1] UGC-DAE Consortium for Scientific Research, University Campus, Khandwa Road, Indore 452001, Madhya Pradesh, India
[2] School of Studies in Chemistry & Biochemistry, Vikram University, Ujjain 456010, Madhya Pradesh, India

E-mail: okram@csr.res.in and vikash@csr.res.in

Received 11 July 2019, revised 8 November 2019
Accepted for publication 9 December 2019
Published 6 January 2020

Abstract

Clear influence of particle size, surfactants and dispersion medium on surface plasmon resonance (SPR) features of Ag nanoparticles (NPs), synthesized in thermal decomposition method, in the broad range of ultraviolet (UV) radiation, critical for many potential applications such as a photocatalyst, UV-sensor and detector, has been demonstrated here. It involves adsorbate coverage, interparticle distance or agglomeration, surface charge density and solvent refractive index (μ). NP agglomeration and surface charge density in solvents of varying μ have been studied systematically through zeta-potential (ζ) and hydrodynamic diameter (HD) using dynamic light scattering (DLS). The main SPR feature found at 316 nm in 31.5 nm NPs shifts to 320 nm in 15.1 nm NPs. The peak at 320 nm in air shifts to 259, 261 and 277 nm in polar solvent methanol, deionized water and ethanol, respectively and to 255, 275 and 282 nm in non-polar solvent n-hexane, benzene and toluene, respectively. In general, the decrease in particle size and increase in μ of solvents show red-shift. Curiously, a number of peaks up to seven in these solvents that are attributed to charge-transfer mechanism and change in inter-particle interaction of the NPs turning from a single peak of SPR in air has been observed for the first time. A model for re-adjustment of Fermi level (E_F) of Ag NP and the highest occupied molecular orbital (HOMO) and lowest unoccupied molecular orbital (LUMO) to explain them has also been used. Moreover, the Drude model for shift in the position of SPR in these NPs is only applicable in non-polar solvents, not in polar solvents. Such novel features will be potential candidates for various applications.

Keywords: silver nanoparticles, surfactant, surface plasmon resonance, particle size, dispersant

S Supplementary material for this article is available online

(Some figures may appear in colour only in the online journal)

Introduction

The collective oscillations of charged density between metal surface and dielectric matrix, known as surface plasmon resonance (SPR), have always attracted much attention in research due to their excellent sensitivity to many surface properties [1]. Particularly, in nanoparticles (NPs), these oscillations are localized or confined in a small region, known as localized SPR (LSPR), resulting in enhancement of the amplitude of electro-magnetic field and hence strong resonance effects. However, these are hindered if dielectric loss is large. Ag NPs get much attention in this context since they have lowest loss in the visible spectrum compared to other plasmonic materials, and hence less attenuation of SPR [2]. In addition, their excellent catalytic properties, high electrical and thermal conductivity makes them promising candidate for many potential

applications [2, 3] such as plasmon-enhanced light harvesting and photocatalysis [1, 2], chemical, biological sensing and optics-based sensing [3, 4, 9], surface-enhanced Raman spectroscopy [18] and nanoelectronics and biomedical applications [3–10].

For example, Shen *et al* showed that Ag NPs dispersed in water can be used as ink for inkjet printer [8]. Sheldon *et al* reported that noble metal nanostructures have plasmoelectric potential that can convert light into electrical energy [7]. Recently, Frazer reported that Ag NPs can be used for treatment of human immunodeficiency virus (HIV) [11]. It is also found that ion, salt and NPs of Ag can be utilized in numerous consumer products and medical devices, due to its excellent antibacterial action [12]. In fact, many physical and chemical parameters such as particle size, size distribution, shape, inter-particle interaction or agglomeration of NPs, dielectric matrix or adsorbent/s and solvent refractive index [13–16] can influence SPR. Size-dependent modifications on SPR such as shifting, broadening and damping in Ag NPs are more visible below the mean free path of electrons (52 nm) [17]. Solution phase synthesis of NPs is more efficient in this and easier one to tune the particle size, shape, size distribution and dielectric environment using variety of surfactants. However, synthesis of metal NPs is very challenging due to their tendency to quick oxidation.

The SPR in thin film nanowires and NPs of Ag is widely reported [1, 4, 17–21]. Several reports exist towards long wavelength (red-shift) [1, 13, 14] as well as towards short wavelength (blue-shift) [1, 22, 23] along with different positions of plasmon modes. For example, Peng *et al* showed blue-shifts in SPR, as size decreases from 20 to 12 nm and then turns over in red-shift near 12 nm in ensembles of monodispersed silver nanospheres stabilized with oleylamine (OA) ligands in hexane. Scholl *et al* reported the blue-shift in main characteristic feature of SPR with decrease in particle size from 20 to 2 nm in single Ag NP [17]. The blue-shift and damping in SPR with a decrease in film thickness is also reported [24]. Ding *et al* theoretically calculated SPR peak positions near 3.7 eV (333 nm) and 7.5 eV (165 nm) using Monte Carlo simulation method by means of reflection electron energy loss spectrum. The prominent surface plasmon peak overwhelms the feeble bulk plasmon feature near 333 nm, but peak near 165 nm exhibits both surface-and bulk-excitation contribution. It is found that the bulk plasmon feature is overwhelmed by the intense surface plasmon feature in the measured spectrum peak at about 3.7 eV. Yoon *et al* reported two absorption peaks at 440 and 580 nm in nanopatterned metal thin film [21]. The main SPR peaks for Ag nanowires of diameters of 30–35 nm and 20–22 nm is in the range of 370–372 and 365–366 nm, respectively [19, 25]. Recently, Jang *et al* reported main SPR around 361 nm in 15 nm nanowires [26]. They found blue-shift in SPR peak with decrease in diameter of nanowire from 28 nm to 15 nm. Wang *et al* reported the blue-shift in Ag nanocubes with decrease in size of cube [22].

However, these investigations have not yet performed the possible tuning of SPR peak feature of metal surface and dielectric matrix using several solvents. They have been implemented successfully in this work using Ag NPs of

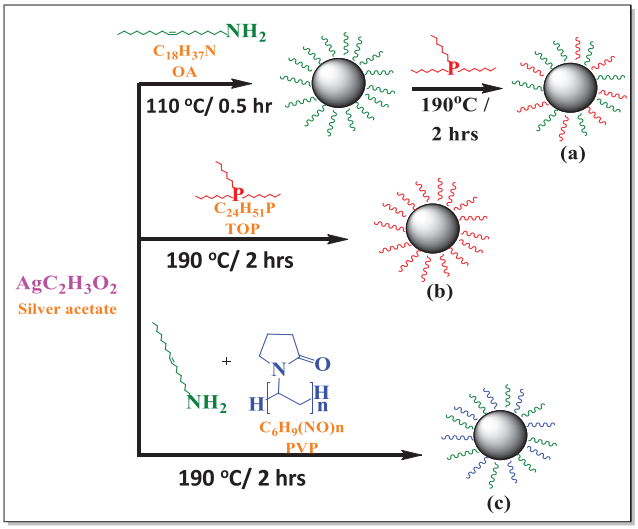

Figure 1. Schematic representation of preparation and surface functionalization of Ag NPs using silver acetate, OA and TOP, (b) TOP only and (c) OA and PVP.

Scherrer size ranging from 15.1 to 33.4 nm, synthesized using silver acetate, OA, trioctylphosphine (TOP) and polyvinylpyrrolidone (PVP) in very a simple and reproducible thermal decomposition method. We therefore demonstrate here the modification in dielectric environment around particles that led to exhibition of multi-peak SPRs observed first time and to changes in stability of the NPs. Their dispersion properties such as zeta potential (ζ), hydrodynamic diameter (HD) and mobility in various solvents are studied using dynamic light scattering (DLS). UV–Visible spectroscopy is used to study effect of particle size, inter-particle interaction or agglomeration, dielectric environment or cappants and solvent refractive index on SPR. In contrast to blue-shift SPR in air, it is found to be red-shifted, damped and narrower with decrease in particle size. Asymmetry at low wavelength side in the main SPR peak, with decrease in particle size, is also observed. Similarly, increase in refractive index (μ) of the solvent leads to red-shift in both polar and non-polar solvents. An attempt has also been made to assess the applicability of Drude model for shift in main SPR peak in polar and non-polar solvents.

Experimental

Typically, 1 ml preheated TOP (90%, Sigma Aldrich) at 210 °C is added in a solution of 1.5 g silver acetate (≥99%, Alfa Aesar) and 10 ml OA (70%, Sigma Aldrich), already degassed at 110 °C for 30 min. The resulting solution is further heated at 190 °C for 2 h under argon atmosphere and cooled to 30 °C, and centrifuged in n-hexane to extract and wash the NPs. The washing is performed three to four times to remove the excess OA and TOP, not bound on NPs surface. The particles dried at 60 °C in vacuum drier are used for various characterizations. This sample was coded as Ag1. Samples synthesized, with 3 ml, 5 ml and 10 ml of TOP, respectively, with other reaction conditions remaining the same, are coded Ag2, Ag3 and Ag4. Two additional samples are prepared in 8 ml and 12 ml of TOP *only* at 190 °C for 2 h under argon atmosphere; they are coded

Table 1. Sample synthesis conditions, particle size, SPR peak positions (in air) and lattice parameter.

Sample	TOP (ml)	OA (ml)	PVP (gram)	XRD size (nm)	TEM size (nm)	SPR peak position (nm)	Lattice parameter (Å)
Ag1	1	10	—	31.5 ± 0.3	—	316	4.083 66 ± 0.000 08
Ag2	3	10	—	28.9 ± 0.2	29.1 ± 1.2	318	4.088 48 ± 0.000 29
Ag3	5	10	—	24.7 ± 0.2	25.3 ± 0.9	318	4.089 19 ± 0.000 37
Ag4	10	10	—	15.1 ± 0.3	15.9 ± 1.1	320	4.087 73 ± 0.000 50
Ag5	8	—	—	29.6 ± 0.4	60 ± 2	318	4.085 66 ± 0.000 28
Ag6	12	—	—	24.6 ± 0.2	—	320	4.086 31 ± 0.000 31
Ag7	—	10	0.25	33.4 ± 0.3	41.7 ± 1.2	318	4.087 22 ± 0.000 42

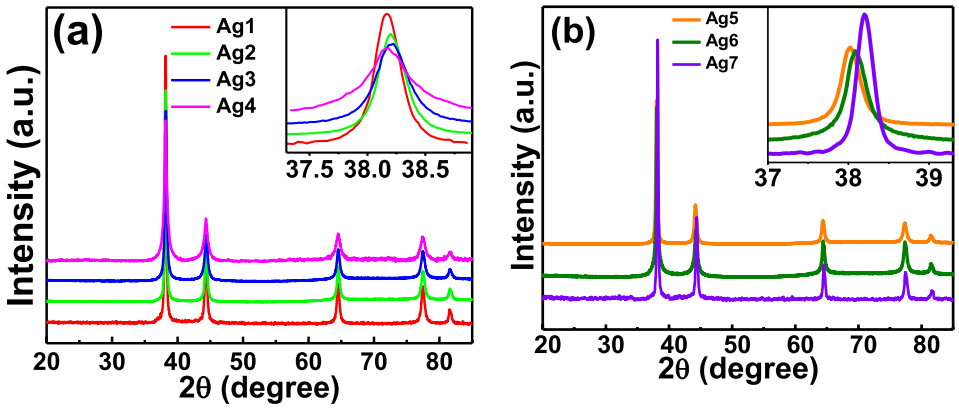

Figure 2. XRD patterns (a) Ag1, Ag2, Ag3 and Ag4, and (b) Ag5, Ag6 and Ag7.

as Ag5 and Ag6, respectively. Another sample, coded as Ag7, was also synthesized in a mixture of 10 ml of OA and 0.25 gram of PVP (K 30) with other heating conditions remaining the same. They were synthesized thus to see the effect of adsorbates and surfactants on SPR. Schematic of synthesis of NPs and preparation conditions are shown in figure 1 and table 1, respectively.

X-ray diffraction (XRD) data are collected using a D2 Phaser x-ray diffractometer with Cu K_α radiation (1.54 Å) in an angle range (2θ) from 20° to 90°. TEM and FESEM measurements are performed using TECHNAI-20-G^2 (200 KV) and FEI Nova nanosem450 on drop-casting the well-sonicated dispersion of NPs in ethanol on carbon-coated TEM grids and drop-casted several times on glass slides, respectively. To confirm coating on the surface of NPs with surfactants, we did Fourier transformed infrared (FTIR) spectroscopy using an FTIR spectrometer (Bruker, Vertex 70), and valence state is examined using x-ray photoelectron spectroscopy (Al-K_α, $\lambda = 0.834$ nm) after argon ion sputtering. The UV–Visible data in diffused reflectance mode are collected using Perkin Elmer Lambda 950 in the wavelength range 200 nm to 800 nm with resolution of 0.05 nm and wavelength accuracy of ±0.08 nm. Particle size and zeta potential (ζ) measurements using a DLS-based Zeta/NP analyser (NanoPlus-3) are performed after thorough sonication of the NPs dispersed in various solvents viz., methanol, deionized water, ethanol, n-hexane, benzene and toluene to study the effect of dielectric environment with different refractive indices and stability of particles. Concentration of NPs added is 0.1 mg ml^{-1} in each case.

Result and discussion

X-ray diffraction

XRD patterns of Ag1, Ag2, Ag3, Ag4, Ag5, Ag6 and Ag7 are shown in figure 2. Ag1 exhibits peak positions at $2\theta = 38.40°$, 44.20°, 64.36°, 77.33°, 81.47° due to reflections from (1 1 1), (2 0 0), (2 2 0), (3 1 1) and (2 2 2) planes, respectively. They confirm the face-centered cubic (fcc) phase of Ag (JCPDS# 893722) without any impurity peak. Similar results are evident from the XRD patterns of other remaining samples indicating that their respective crystal structure is fcc phase without any impurity phase. Notably, the peaks are broadened with increase in concentration of TOP, which indicates reduction in particle size. The average particle size of NP samples is evaluated using Scherrer's formula (table 1).

In addition, it is appropriate to point out that peak positions are slightly shifted to lower or higher angles, which are due to use of sample pellets instead of powdered ones. This can lead to the shift generally randomly since any change in distance between sample surface and detector can be different. Generally, genuine higher or lower angle shift in XRD peak indicates the lattice contraction or lattice expansion, respectively. In order to remove this discrepancy, we have done Rietveld refinements of XRD data using Fullprof_suite software and calculated the lattice parameters as shown in figure 3, and obtained lattice parameter (a) is listed in table 1. The lattice parameter increases from Ag1 to Ag3 indicating that lattice is expanded with decrease in particle size. However, lattice parameter is found to be smaller in Ag4 than that of Ag2 and Ag3 but larger than that of Ag1. This situation seems

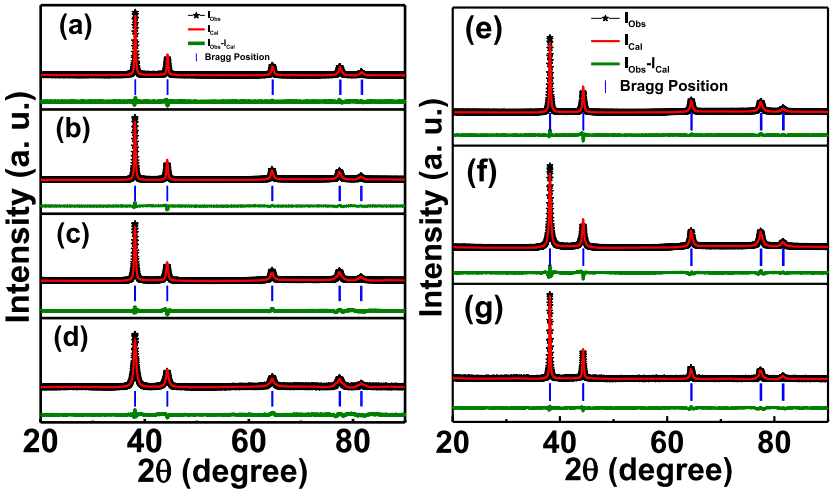

Figure 3. Rietveld refinement data of (a) Ag1, (b) Ag2, (c) Ag3, (d) Ag4, (e) Ag5, (c) Ag6 and (e) Ag7.

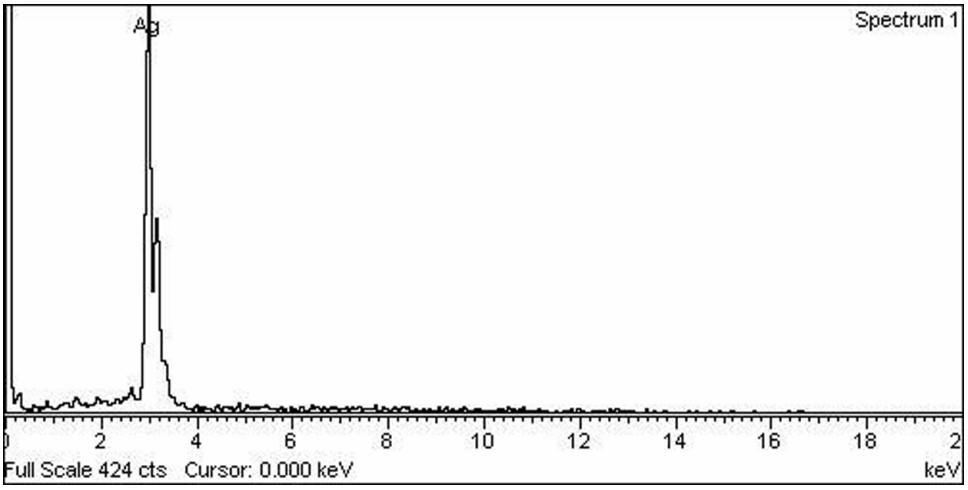

Figure 4. Energy dispersive x-ray spectrum of Ag4.

to show that there is limit in the lattice expansion. Similarly, the lattice parameter increases with decrease in particle size in samples prepared in pure TOP i.e. Ag5 and Ag6, and Ag7. This is in line with Ni NPs [27].

EDX and XPS study

Figure 4 shows the EDX spectra of Ag4, which is found to be the same as those of Ag5 and Ag7. This indicates the peak related to Ag without any impurity peak. Quantitatively, 100% Ag content is found, since others due to surfactants are undetectable. To see the valence state or any oxidation of NPs, XPS measurements are performed on Ag4. Fitted spectra using XPSPEAK4.1 software of C 1s, O 1s and Ag 3d along with survey scan are shown in figure 5; fitted parameters are presented in table S1 (stacks.iop.org/JPhysCM/32/145302/mmedia). The two deconvoluted peaks near at 285.1 eV and 286.7 eV in C 1s correspond to C–C and C–O, respectively of OA, TOP or acetate (figure 5(a)).

The two deconvoluted peaks around 531.8 eV and 532.9 eV of O 1s (figure 5(b)) attributed to low coordination bonding of O–H and C–O of acetate (–COOH), not due to presence of Ag^{+1} or Ag^{+2} states since oxides generally show narrower peak widths and give rise to two well-resolved peaks in O 1s [28]. Furthermore, two well-resolved peaks around 368.3 eV and 374.3 eV in Ag 3d corresponding to spin–orbital components, Ag $3d_{5/2}$ and Ag $3d_{3/2}$, respectively, are observed (figure 5(c)). The peak around 368.3 eV and the separation between spin–orbital components found to be 6.0 eV with intensity ratio of about 1.49, consistent with that of theoretical value of 1.5, are evidence for metallic Ag [28]. Therefore, EDX and XPS results confirm the single phase of metallic Ag NPs and therefore oxide of Ag is ruled out.

In survey scan (figure 5(d)), the two sharper peaks near 368.3 eV and 374.3 eV are assigned to the $3d_{5/2}$ and $3d_{3/2}$, respectively of Ag, and two well-resolved peaks near 335.5 eV and 353.4 eV are appeared due to $4d_{5/2}$ and $4d_{3/2}$, respectively of Au (figure 5(d), right inset). The peaks of Au also appear in the survey scan as the sample was mounted on gold plate; two peaks near 84.0 eV and 87.7 eV due to spin orbit splitting components $4f_{7/2}$ and $4f_{5/2}$ and 547.4 eV and 643.5 eV due to $4p_{3/2}$ and $4p_{1/2}$, respectively of Au are also seen. Two low intensity peaks near 573.2 eV and 604.3 eV due to $3p_{3/2}$

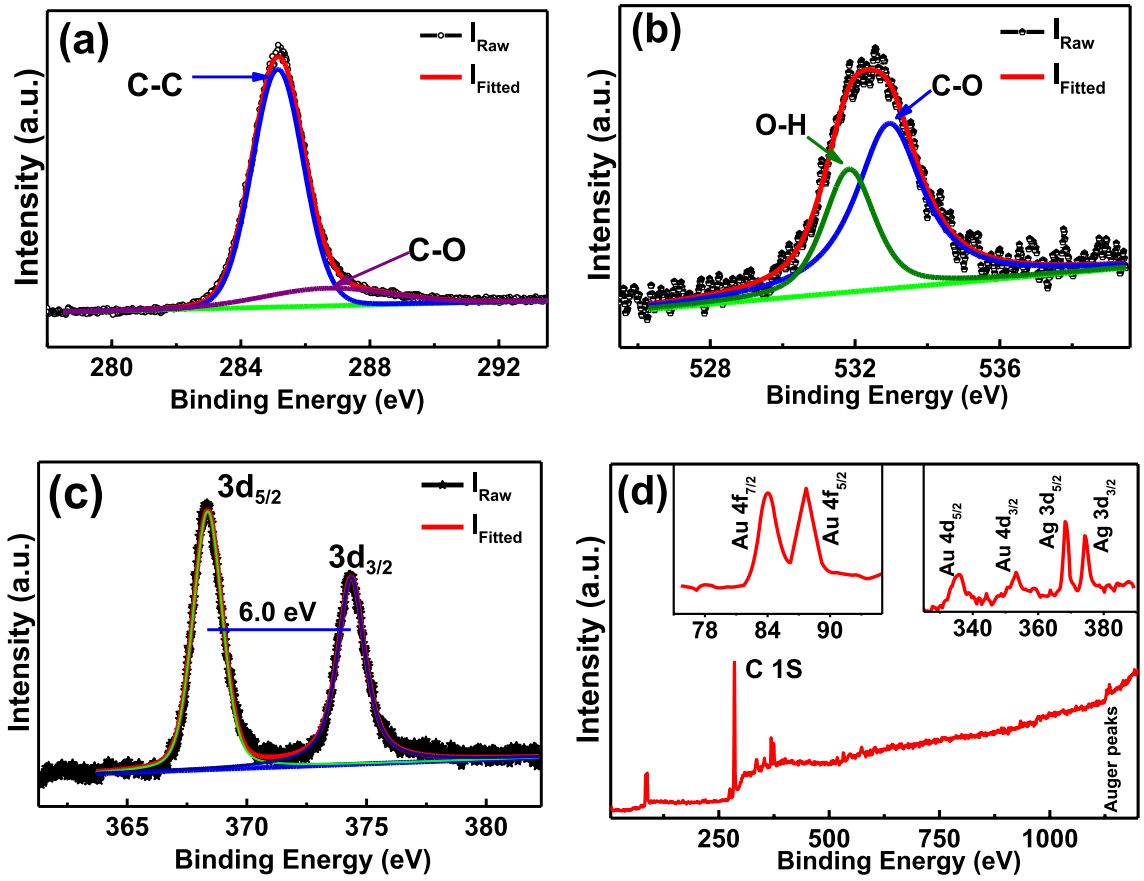

Figure 5. XPS spectra of (a) C 1 s, (b) O 1s, (c) Ag 3d and (d) survey scan of Ag4; insets: expanded portion of the regions as indicated.

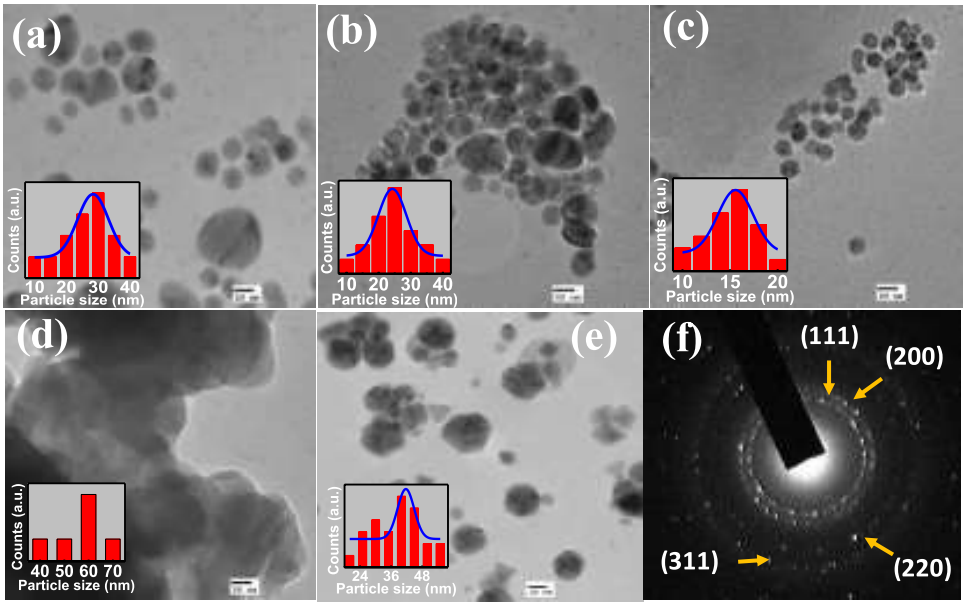

Figure 6. TEM micrographs ((a)–(e)) of Ag2, Ag3, Ag4, Ag5 and Ag7, and selected area electron diffraction (SAED) pattern of Ag2 as representative SAED pattern. Inset: respective size distribution plots. Scale bar of all images is 20 nm.

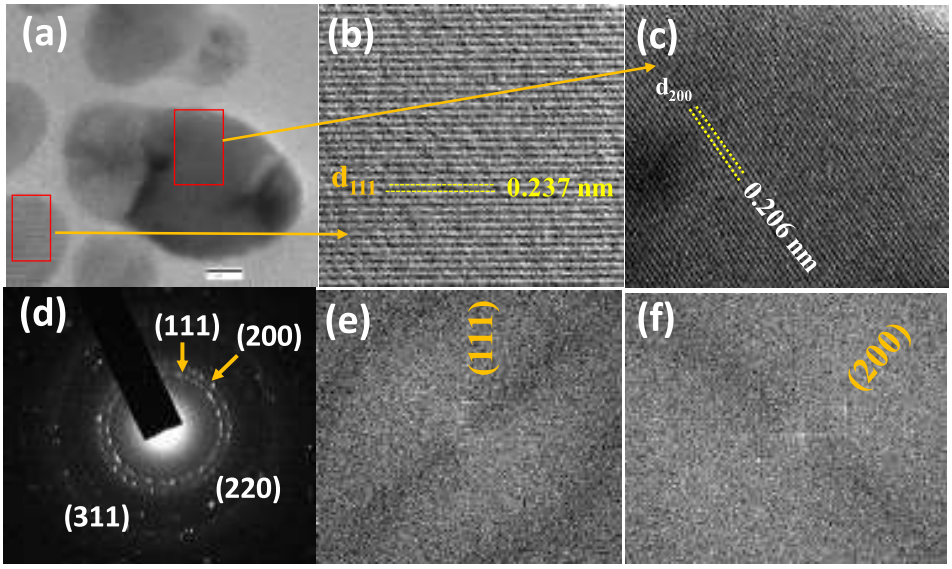

Figure 7. HRTEM micrographs ((a)–(c)), (d) SAED and (e), (f) FFT of plane (1 1 1) and (2 0 0), respectively of Ag2. Scale bar of (a) is for 5 nm.

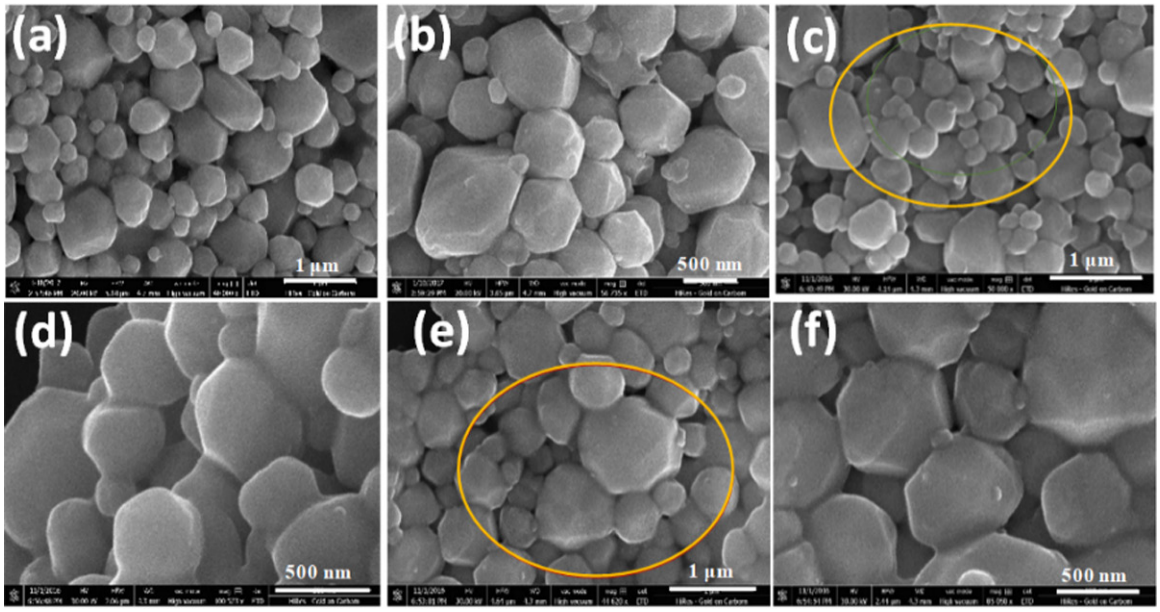

Figure 8. FESEM micrographs of Ag4 at different scales in powder form on carbon tape (a) and (b), dispersed in n-hexane and drop-casted on glass slide (c), (d) and ethanol and drop-casted on glass slide (e) and (f). The scale bar is 1 μm in (a), (c), (e) and 500 nm in (b), (d), (f).

and $3p_{1/2}$, respectively for Ag are also seen. Two peaks at 1128.8 eV and 1134.7 eV are associated with auger peaks in Ag due to Al K_α source.

HRTEM and FESEM study

The TEM micrographs of Ag2, Ag3, Ag4, Ag5 and Ag7 and their size distributions as insets along with selected area electron diffraction (SAED) pattern of Ag2 as representative SAED pattern are shown in figure 6. The size distribution of NPs is found to be between 10 to 40 nm, 10 to 40 nm and 10 to 20 nm with average particle size around 29.1 ± 1.2 nm, 25.3 ± 0.9 nm, 15.9 ± 1.1 nm in Ag2, Ag3 and Ag4 as shown in figures 6, insets (a)–(c), respectively. The decrease in particle size and enhanced monodispersity of NPs with increase in TOP are found such as NPs of Ag4 are reasonably monodispersed (figure 6(c)) compared to Ag2 (figure 6(a)). The average particle size is ~60 nm for Ag5 (figure 6(d)). Therefore, NPs prepared in pure TOP seem to be more agglomerated and bigger in size compared to that prepared in combination of OA and TOP (figure 6(c)).

The shape of NPs prepared in TOP and combination of OA and TOP appears generally spherical. The particle size of NPs obtained from XRD and TEM are nearly the same in Ag2, Ag3 and Ag4 (table 1). TEM size of Ag5 (60 nm) found to be significantly larger than XRD size due to agglomeration of smaller NPs (table 1). This is attributed to the smaller crystallites (XRD size) being agglomerated into bigger size particle

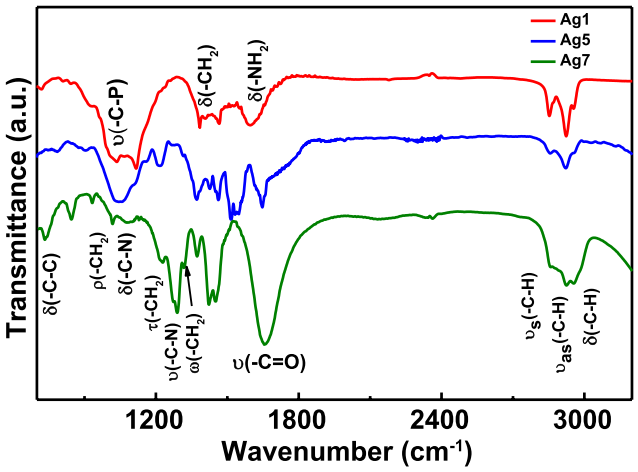

Figure 9. FTIR spectra of Ag1, Ag5 and Ag7.

in TEM. Similarly, very random triangular, rectangular, hexagonal and spherical shapes of NPs are found in Ag7 (figure 6(e)) with an average size of about 41.7 nm, which is significantly larger than the XRD size (table 1). Finally, SAED pattern of Ag2 is shown in figure 6(f) as representative SAED pattern that confirms the fcc structure seen in XRD (figure 2).

High resolution TEM data for Ag2 are shown in figures 7(a)–(c). SAED patterns clearly indicates the reflection from (1 1 1), (2 0 0), (2 2 0) and (3 1 1) planes of fcc phase of Ag NPs (figure 7(d)). The interplanar spacing (d) around 0.237 nm and 0.206 nm corresponding to (1 1 1) and (2 0 0) planes, respectively are obtained from HRTEM (figures 7(b) and (c). The fast Fourier transformed (FFT) patterns of these planes are shown in figures 7(e) and (f). These results prove that Ag2 is fcc Ag NPs.

FESEM micrographs of Ag4 in powder form and after dispersing in ethanol or n-hexane and consequent drop-casting on glass slides are shown in figure 8. The measurements on dispersed NPs have been performed to see the effect on morphology and inter-particle interactions in comparison with powder sample. Morphology of NPs found to be hexagonal-like in powder form as well as in n-hexane and ethanol. The hexagonal-like shape here compared to nearly spherical shapes in TEM (figure 6(c)) could be due to extra agglomeration when the particle density and thickness is more in FESEM. However, it can be seen that interparticle distance is less in n-hexane (figures 8(c) and (d)) and ethanol (figures 8(e) and (f)) compared to powder (figures 8(a) and (b)), and inter-particle distance is more in ethanol compared to n-hexane (figures 8(c) and (e). Notably, the identical morphology of NPs before and after dispersing in ethanol and n-hexane are noted. The variation in inter-particle distance may modify their spatial charge distribution and hence in their SPR, to be discussed later.

FTIR study

FTIR spectra of Ag1, Ag5 and Ag7 are shown in figure 9. The dips due to bending vibration (δ (C=H)), asymmetric stretching (ν_{as} (C–H)) and symmetric stretching (ν_s(C–H)) mode of CH_2 are seen in Ag7 near 2960, 2923 and 2851 cm^{-1}, respectively [29–32]. A sharp dip near 1656 cm^{-1} assigned to stretching vibration of C=O (ν (C=O)) of PVP, and dips at 1457 and 1418 cm^{-1} are associated with scissoring vibration of CH_2 group of PVP [33, 34]. Dips near 1370 and 1315 cm^{-1} are assigned to CH_2 bending ($\delta(CH_2)$) and wagging vibration ($\omega(CH_2)$), respectively, and 1288 cm^{-1} is due to C–N stretching vibration (ν (C–N)) [33,34]. The vibrations 1221 and 1013 cm^{-1} are appeared due to CH_2 twisting ($\tau(CH_2)$) and rocking ($\rho(CH_2)$), respectively, and 1089 cm^{-1} is due to bending vibration of C–N (δ (C–N)) of OA. A vibration near 728 cm^{-1} is also seen due to bending vibration of –C–C (δ(–C–C)). Similar vibrations (δ (C=H), (ν_{as} (C–H) and ν_s(C–H)) of CH_2 are also seen in Ag1 and Ag5 with slightly shifted positions [29–32]. The bending vibration of NH_2 ($\delta(NH_2)$) appeared around 1595 cm^{-1} in Ag1, which is not clearly visible in Ag7, is due to intense stretching vibration ν(C=O) of PVP [33, 34]. Dips near 1065 and 1070 cm^{-1} are due to C–P modes of TOP in Ag1 and Ag5, respectively [29–32]. These results indicate that Ag1, Ag5 and Ag7 are coated with OA-TOP, TOP and OA-PVP, respectively.

DLS study

Intensity distribution of HD of Ag4 in different solvents at pH = 7 are shown in figure 10. HDs in methanol in the first run 250 and 25 930 nm turn 257 nm and 26 730 nm in the second run. They are 145 nm & 13 165 nm and 290 nm & 13 970 nm in DIW, 160 nm & 13 450 nm and 170 nm & 15 860 nm in ethanol, 38 nm, 200 nm & 6820 nm, and 42 nm & 2752 nm in n-hexane, respectively. They are indicative of having groups of particles corresponding to the peaks with a contrast in n-hexane to the usual observations that they get agglomerated into bigger ones with time delay. The fragmentation of bigger particles into smaller ones appears in n-hexane. However, in benzene and toluene, there is a single peak each at 12 210 nm and 15 080 nm, respectively. Notably, while two peaks each in methanol, DIW and ethanol in both runs are found with increased values in the second run, there are three peaks in the first run and two peaks in the second run in n-hexane with increased value in the smallest value but reduced value of the bigger value in the second run. Such results are very intriguing since dispersion characteristics of a particular NP is so divergent depending on the type of dispersant such as these. They will influence significantly the zeta potential values and SPR behaviour of the NPs in these dispersants as presented below.

Figure 11 shows the intensity distribution of ζ of Ag4 in various solvents at pH = 7. It is interesting to note that five peak values of ζ at 0.9 mV, 14.60 mV, 22.70 mV, 33.60 mV and 82.70 mV in the first run turn out to be three peaks at 13.45 mV, 26.80 mV and 74.50 mV in the second run in methanol. They are indicative of having groups of particles corresponding to them. They get agglomerated very fast into bigger ones (as reduced ζ is indicative) with time delay that appear as reduced number of peaks. Two peaks at −37.23 mV & −32.30 mV in the first run remains to be two peaks at −36.02 mV and −28.30 mV in the second run in DIW. Two

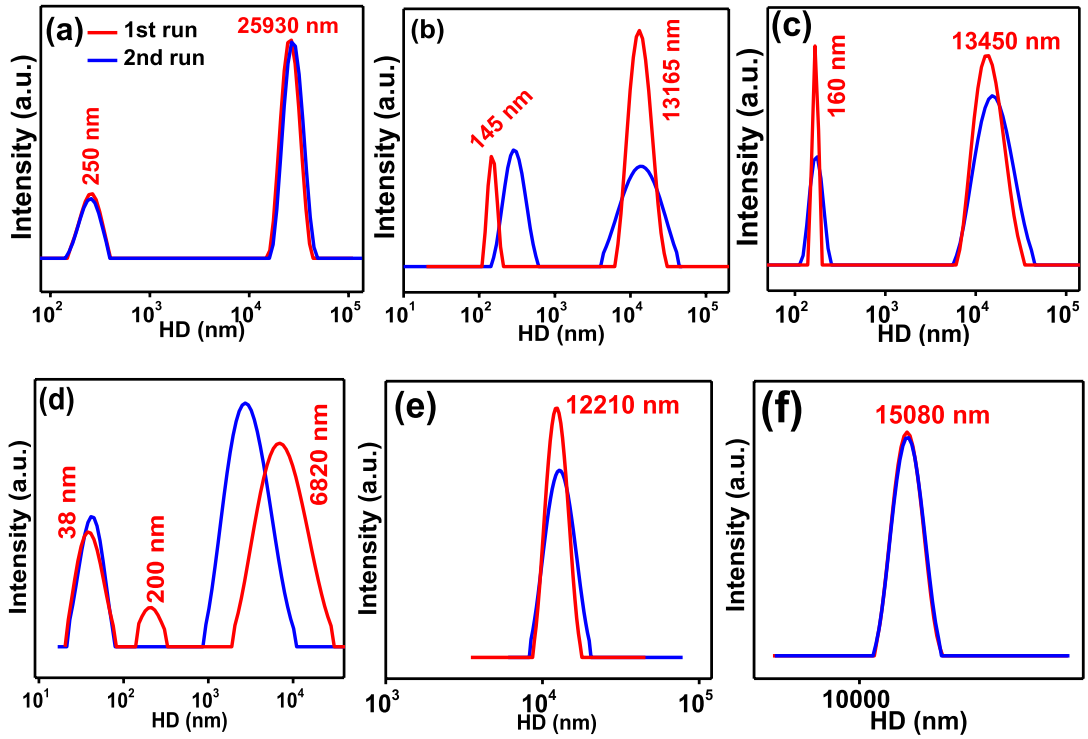

Figure 10. Intensity distribution of HD of Ag4 in (a) methanol, (b) deionized water, (c) ethanol, (d) n-hexane, (e) benzene and (f) toluene. The red and blue curves are first run and second run, respectively as shown in (a).

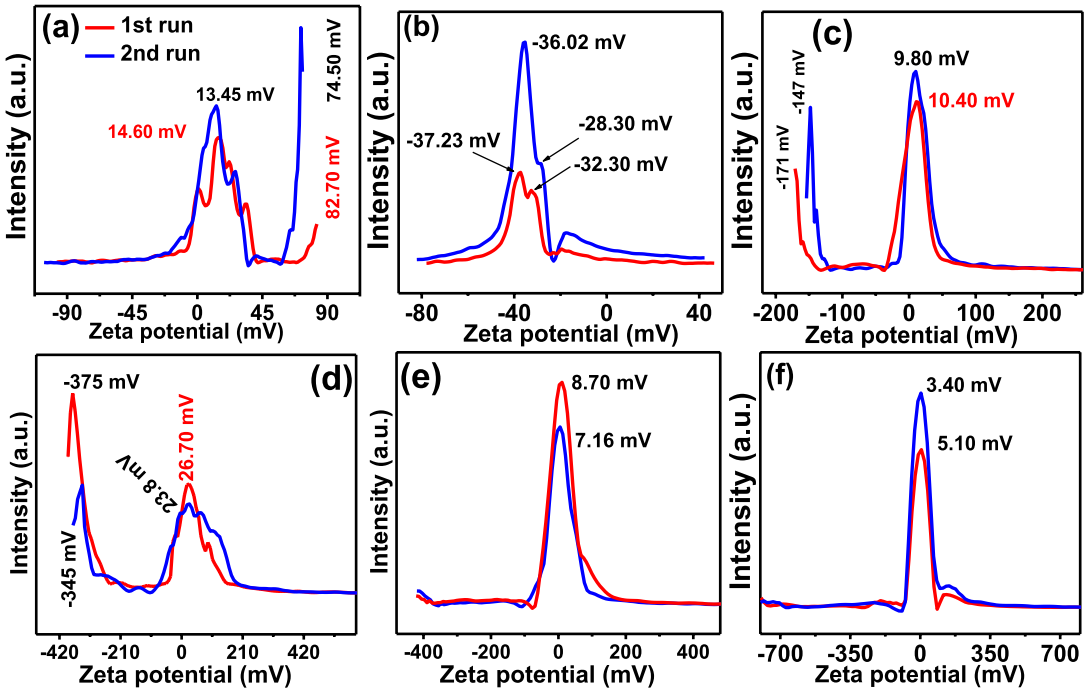

Figure 11. Intensity distribution of zeta-potential of Ag4 dispersed in (a) methanol, (b) deionized water, (c) ethanol, (d) n-hexane, (e) benzene and (f) toluene. The red and blue curves are first run and second run, respectively as shown in (a).

peaks at 10.40 mV and −171 mV turn to be two peaks at 9.80 mV and −147 mV in the second run in ethanol. Four peaks at 89.80 mV, 26.70 mV, 26.94 mV and −375 mV in the first run became three peaks at 67.90 mV, 22.50 mV and 345 mV in the second run in n-hexane. Similar explanation holds true as in methanol. One peak at 8.70 mV in the first run remains to be one peak at 7.16 mV in benzene. Similarly, in toluene, the single peaks are at 5.10 mV and 3.40 mV, respectively. Notably, bigger clusters might settle at the bottom of cuvette, and their mobility will be lower compared to smaller particles. As a consequence ζ is expected to decrease, since it is proportional to mobility [35]. It can qualitatively be seen that smaller

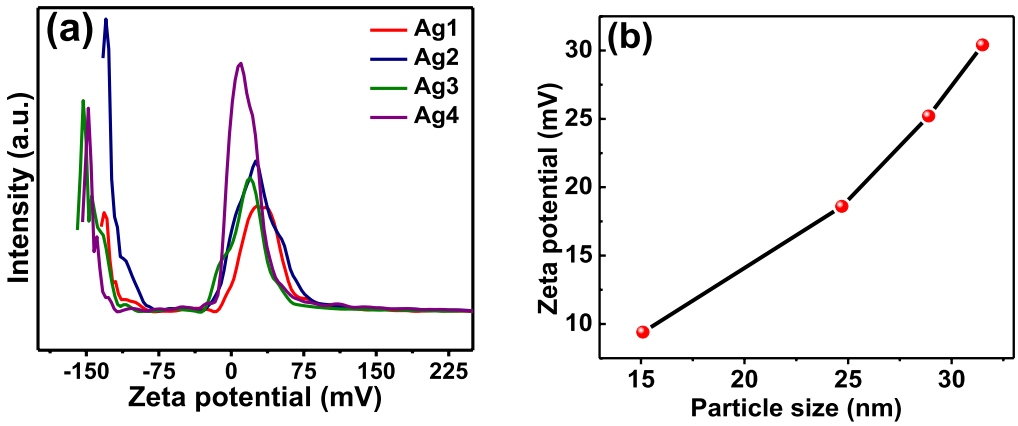

Figure 12. (a) Zeta potential of Ag1, Ag2, Ag3 and Ag4 in ethanol, and (b) size dependence on zeta potential in ethanol.

particles move rather faster compared to bigger particles and hence zeta potential should be higher for smaller particles. This is consistent with larger HD and smaller ζ in the second run compared to the first run, which is due to agglomeration of NPs with time [16].

These data are therefore very fascinating as they reflect very complex nature of the presence of different kinds of agglomerated particles which are not distinguishable in HDs. This would be the reason why even though only two peaks are seen in both the runs in HDs, there are five peaks in the first run but three peaks are seen in the second of the ζ plot for methanol. Complexity reduces in n-hexane. Similarly, in DIW and ethanol with two peaks each and to the least in benzene and toluene with a single peak each. The lager ζ corresponds to smaller particles and smaller ζ corresponds to agglomerated clusters as found in HD data. Interestingly, only one peak in benzene and toluene is found, which is consistence with their one size distribution peak in HDs (figure 10). Also, two well-separated peaks in methanol, ethanol, DIW and n-hexane can be seen in ζ. Moreover, the splitting in main peak in methanol, DIW and n-hexane can clearly be seen, which is more in methanol and n-hexane compared to DIW. Notably, NPs exhibit both negative as well as positive charges or ions within the electrical double layer in ethanol and n-hexane, whereas only positive ions in methanol, benzene, toluene and negative ions in DIW are detected. The reason for negative and positive charges is that, depending on the type of surfactants and dispersant used, the way the polydispersed particles or different shapes interact with the medium decides their charges. Consequently, there may be particles with negative charges as well as positively charged ones. Hence, the zeta potential values. The ζ, HD, mobility and conductivity of ions obtained from DLS measurements are shown in table S2. Generally, Ag NPs are found to be more stable in DIW ($\zeta \geqslant \pm 30$ mV) compared to other solvents.

The average ζ around 30.4 mV, 25.2 mV, 18.6 mV and 9.4 mV for Ag1, Ag2, Ag3 and Ag4, respectively, in ethanol are found (figure 12(a)). The value of ζ decreases as the size decreases, which is illustrated in figure 12(b). The positive value of ζ for Ag1 in ethanol is line with OA and TOP coated Ni NPs [29], and decrease in ζ with increase in quantity of TOP as a medium. The ζ depends highly on the surface chemistry or charge density and functional group per surface area of NPs in comparison of particle size, which is line with earlier report on SiO_2 NPs [36]. This might probably be due to increase in concentration of TOP or increase in phosphine groups on surface of NPs, consequently neutralization of positively surface charges in electrical double layer as seen in Ag1. Therefore, the increase in agglomeration or decrease in zeta-potential is mainly due to increase in coverage of TOP and hence size or its thickness around NPs owing to the modified chemical interactions and surface charge density rather than decrease in particle size (figure 12(b)). Narrower size distribution of ζ in Ag4 than other samples further support its relatively more monodispersity as seen in TEM micrographs (figures 6(a)–(c)).

Influence of particle size and adsorbate coverage on UV–vis spectroscopic response

The diffused reflectance spectra of Ag1, Ag2, Ag3, Ag4, Ag5, Ag6 and Ag7 are shown in figure 13. Dips found to be near 220, 320, 378, 454, 498 and 554 nm in Ag4 are denoted by P1, P2, P3, P4, P5 and P6, respectively (figure 13(d)). They appear at 220, 316, 378, 488 and 558 nm in Ag1 (figure 13(a)), 220, 318, 378, 488 and 558 nm in Ag2 (figure 13(b)), 220, 318, 378, 490 and 556 nm in Ag3 (figure 13(c)) and 220, 318, 374, 484 and 562 nm in Ag5 (figure 13(e)), 220, 320, 375, 450, 498 and 558 nm in Ag6 (figure 13(f)) and 218, 318, 378 and 500 nm in Ag7 (figure 13(g)). Peak P1 position in Ag1, Ag2, Ag3, Ag4, Ag5 and Ag6, is the same and is attributed to inter-band transition (IBT) in metal NPs [16]. It however shifts to lower wavelength side (blue-shift) by 2 nm in Ag7, which might be due to different dielectric environment or shape of NPs rather than particle size effect, as it does not show size dependence in other samples. Furthermore, P2, P3, P4, P5 and P6 are assigned to SPR in Ag NPs, consistent with earlier reports [1, 4, 17–21] on thin films and NPs of Ag with varying grain sizes, different shapes and dielectric environment. Appearance of P2 is most likely due to dipole SPR, while others are due to quadrupolar and higher multipolar plasmon modes, mainly due to imperfect spherical shape and coupling between dipolar modes of SPR in adjacent NPs [37]. This finding of SPR in UV-regime in Ag NPs is closed to the

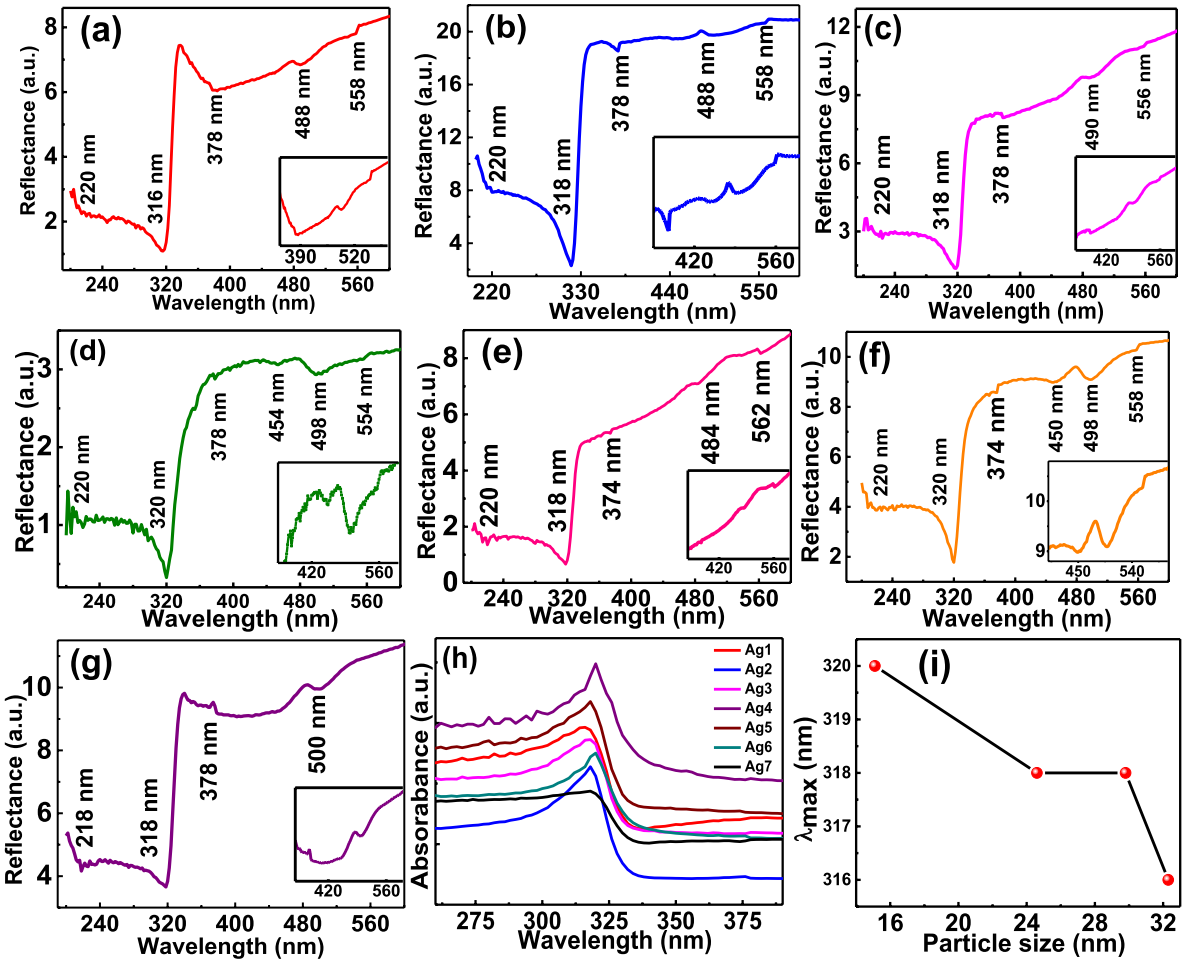

Figure 13. Diffused reflectance spectra in air of (a) Ag1, (b) Ag2, (c) Ag3, (d) Ag4, (e) Ag5, (f) Ag6, (g) Ag7, corresponding absorbance spectra of these samples (h) and (i) wavelength at peak λ_{max} versus particle size plot. Insets: expanded portion of each spectrum for clarity.

bulk plasmon [4]. Nevertheless, most intense and its extended features with variation in particle size, dielectric environment and solvent refractive index, confirmed the dipole SPR, consistent with earlier reports [1, 4, 17–21].

The main SPR peak (P2) found to be red-shifted from 316 to 320 nm with decrease (increase) in particle size (TOP), contrary to blue-shift, is in line with earlier report [1]. Significant asymmetry of P2, at the lower wavelength side, increases with increase in particle size, which may be due to broad size distribution of NPs, as seen TEM data (figure 6). Plasmon modes of NPs may interfere resulting in asymmetry in peak [14, 38]. Furthermore, P2 and P5 are red-shifted in Ag7 compared to Ag1, contrary to blue-shift. Moreover, P6 is completely disappeared in Ag7. These results may be due to different shape, size distribution and dielectric environment rather than particle size. As particle size decreases, P2 and P5 found to be red-shifted, whereas P6 is blue-shifted in Ag1, Ag2, Ag3 and Ag4. Moreover, while P3 does not show any size dependence, P4 is present in Ag4 and Ag6 only. Similarly, P2 and P5 are red-shifted and P6 is blue-shifted, while P3 did not shift with decrease in particle size. These results are respectively consistent with earlier reports of red-shift [1, 14] and blue-shift [23] in plasmon modes for Ag NPs with decrease in particle size. Furthermore, disappearance of P4 with increase

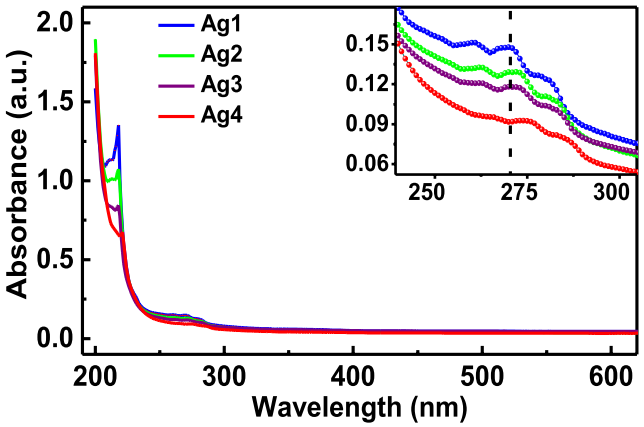

Figure 14. UV–Visible spectra of Ag1, Ag2, Ag3 and Ag4 in ethanol.

in particle size might be due to coupling between plasmonic features, their relevance increases as size decreases, which leads to new feature in smaller NPs [37].

Now, there are two probable situations: first, increase in concentration of TOP, which favours in red-shift and second, decrease in particle size favours of blue-shift. Generally, decrease in particle size in bare NPs may have weaker

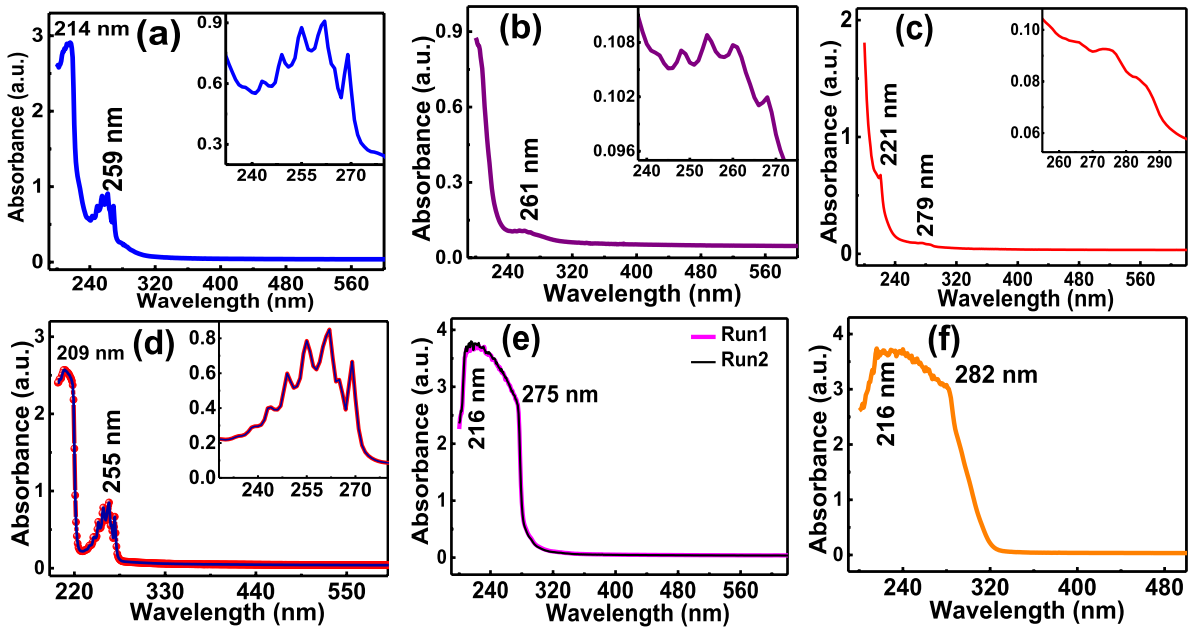

Figure 15. UV–Visible absorbance spectra of Ag4 on dispersion in (a) methanol, (b) DIW, (c) ethanol, (d) n-hexane, (e) benzene and (f) toluene.

interactions of s-d electrons due to finite size and surface effects, which may lead to increase in plasmon energy or blue shift in SPR features [24]. Therefore, the unusual red-shift is most likely to be due to effect of TOP coverage or increase thickness of dielectric matrix, consistent with earlier report [39]. To verify this, UV–Visible measurements were performed on Ag1, Ag2, Ag3 and Ag4 in ethanol (figure 14). There is clear increase in red-shift P2 with increase in TOP concentration. On the contrary, P2 is blue-shifted to near or less than 275 nm and split into three peaks in ethanol compared to air 316–320 nm (figure 13(i)) as illustrated in inset of figure 13 that will be discussed later further. It is gradually broadened, damped and become asymmetric as the particle size decreases, consistent with earlier report [38], and our reflectance data (figure 13). Decrease in absolute ζ or reduce surface charge density or increase in agglomeration with decrease in particle size due to more uniform size compared to those of larger particle size samples as reported earlier [29] or as discussed above also corroborate red-shift, consistent with earlier reports [1, 39].

Influence of refractive index of solvent on SPR

In order to find the possible origin of peak splitting and effect of solvent refractive index on SPR, as one peak found in reflectance data in air (figure 13) splits into three independent peaks (figure 14), UV–Visible absorbance spectra of Ag4 in several polar solvents, viz., methanol ($\mu = 1.327$), deionized water ($\mu = 1.3325$) and ethanol ($\mu = 1.3617$), and non-polar solvents, viz., n-hexane ($\mu = 1.3758$), benzene ($\mu = 1.4957$) and toluene ($\mu = 1.4964$) are recorded (figure 15). Peaks around at 214 and 259 nm in methanol, 261 nm in DIW, 221 and 279 nm in ethanol, 209 and 255 nm in n-hexane, 216 and 275 nm in benzene and 216 and 282 nm in toluene are observed. Position of the SPR peak in each sample is determined using Gaussian fitting (figure S1). The first (P1) and second (P2) peaks are related to IBT and SPR, respectively, with modified shape and shifting as found in air. However, remaining peaks (P3, P4, P5 and P6 in figure 13) are not visible in these solvents due to their probable damping with increase in μ [16, 40]. Systematically red-shift in IBT and SPR in both polar as well as non-polar solvent with increase in μ is found, consistent with earlier report [15]. Interestingly, IBT is disappeared in DIW. The SPR is significantly damped and weaker in benzene and toluene, probably due to their higher μ. To see the accuracy of the data, measurements are repeated in n-hexane and benzene; they encouragingly show identical features.

Remarkably, splitting into three, four, five and seven peaks in ethanol, DIW, methanol and n-hexane, respectively, for a single SPR peak exhibited in air has been observed for the first time. They therefore are distinctly different from that observed in Ni NPs [16]. This may be understood by charge transfer mechanism and formation of interface dipole between NPs and surface-bound molecules of the solvent or the adsorbate. When the NPs are dispersed in any medium, the molecules of solvent may adsorb on metal NPs either by physisorption or chemisorption. Consequently, electronic structure of NPs and adsorbate may be modified. Further, charge transfer may take place between NP and adsorbate, if they are chemisorbed, which may affect interface dipoles. The exchange of electrons through chemical bonds will highly depend upon their relative electronegativities. In fact, energy dissipation within the particle is more likely for smaller size NPs (NPs having size smaller than the wavelength of light) compared to bigger NPs. As the particle size increases, re-radiation of the energy by the particle to the surrounding medium is expected to be dominant. Therefore, more localized SPR may be expected due to smaller size NPs compared to bigger NPs. However, it might

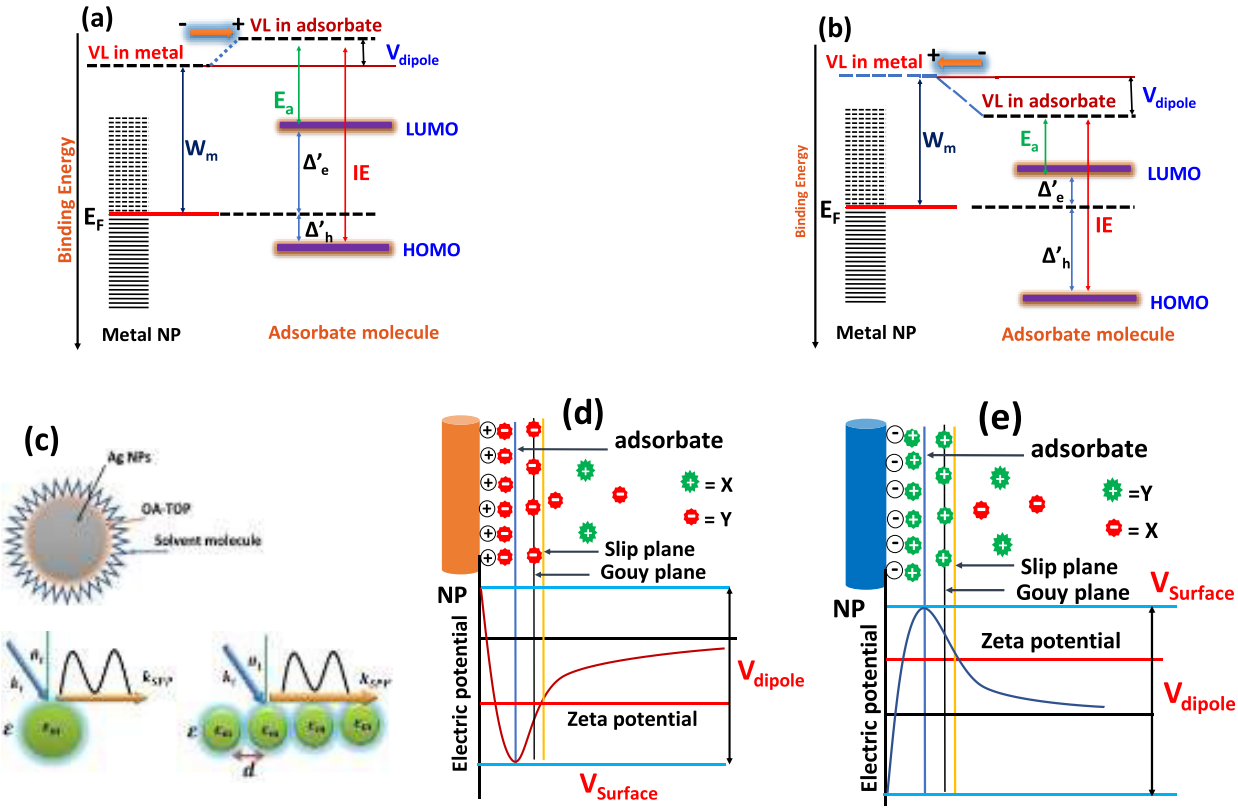

Figure 16. Electronic energy levels at metal/adsorbate interface. (a) Interface dipole directed towards adsorbate and (b) interface dipole directed towards metal, due to VL mismatch. (c) Upper panel: interaction of NP-coated with OA-TOP with solvent molecules and lower panel: effect of interparticle interaction or agglomeration of NPs on surface plasmon polariton. (d) Negatively-charged and (e) positively-charged metal NPs in the medium corresponding to (a) and (b), respectively.

be possible that light is rarely interacted with bigger clusters because of their sedimentation and hence it may be expected that overall effect is mainly governed by smaller NP clusters, which continue to be dispersed. Thus, there are seven, four, three and five split peaks for n-hexane, DIW, ethanol and methanol with HDs of 38, 145, 160 and 250 nm, none in benzene and toluene with HDs of 12 210 and 15 080 nm.

Metal work function (W_m) may be supressed in this due to repulsion between electrons of molecule and metal surface electrons and the direction of the dipole moment will be towards vacuum level (VL) of adsorbate [41]. This further result in abrupt shift in VL from metal to adsorbate molecule interface and hence formation of interface dipole barrier. This means that the energy difference between the Fermi level (E_F) of metal NP and the highest occupied molecular orbital (HOMO) and lowest unoccupied molecular orbital (LUMO) of the solvent molecules may change with respect to a VL alignment situation and charge transfer will depend upon direction and magnitude of interface dipole barrier height. The combined positive pole of interface dipole pointing towards metal NP and negative pole towards surface-bound molecule leads to decrease in the Fermi energy of metal NP and increased HOMO energy of surface-bound molecule by the addition of electrostatic energy and vice-versa [42].

The schematic of negatively and positively charged metal NPs along with formation of interfacial dipole is shown in figure 16. When the surfactant molecules are in contact with metal NP, their electronic energy levels may be modified due to their different work functions or VL. For negatively charged metal NPs, work function may be supressed with direction of dipole towards VL of adsorbate (figure 16(a)). The direction of dipole will be reverting back for positively charged surface of NPs than that of negatively charged surface (figure 16(b)). Therefore, strength of injection barriers for electrons (Δ_e) and holes (Δ_e) may be modified according to direction and height of dipole barrier (V_{dipole}) and hence charge transfer; electronic energy level of NPs is taken discrete due to finite size effects. Schematic representation of interaction of OA-TOP coated NPs with chemically attached molecules of solvent (upper panel) and wavevector of surface plasmon polariton (SPP) or SPR for single NP and ensemble of NPs (lower panel) is shown in figure 16(c). From this we can say that any change in interparticle distance and arrangement of agglomerated particles may highly affect the SPR features [14]. The interaction between negatively charged (figure 16(d)) and positively-charged (figure 16(e)) metal NPs with the medium and corresponding to direction of dipole towards (figure 16(a)) and away from (figure 16(b)) of VL of adsorbate, respectively is shown.

In this context, LUMO ~3.50 eV of methanol is closed to Fermi energy ~5.49 eV of Ag compared to HOMO~ −11.14 eV [43, 44]. While HOMO ~5.39 eV of ethanol is much closed to Fermi level of Ag than LUMO ~ −2.42 eV [43, 44]. Methanol has less electrons injection barrier than ethanol and ethanol

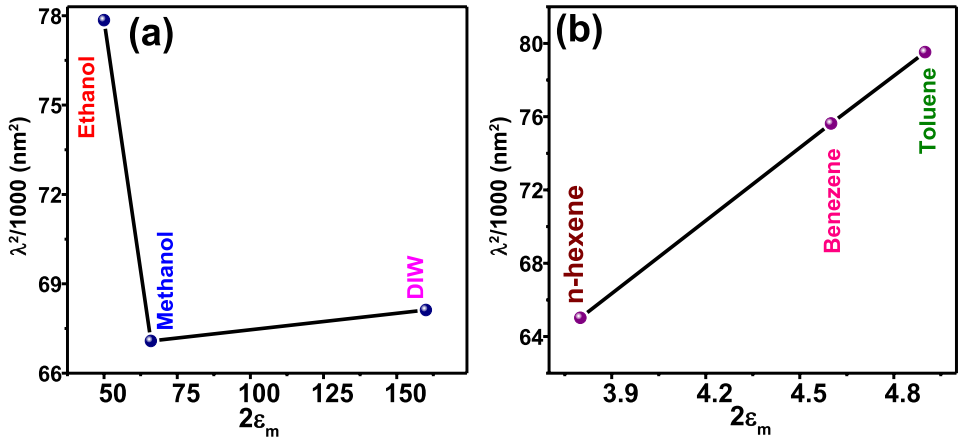

Figure 17. $\lambda^2/1000$ versus ε_m curve of (a) polar solvents and (b) non-polar solvents.

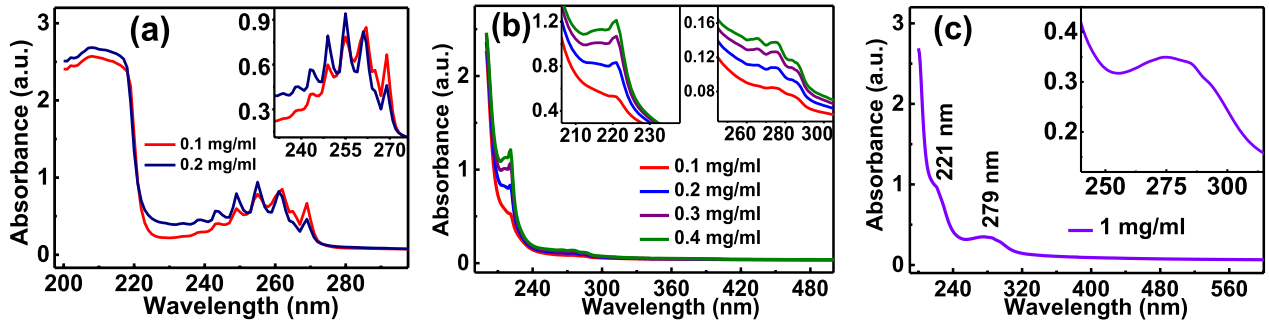

Figure 18. UV–Visible spectra of Ag4 with varying concentrations in (a) n-hexane (0.1 and 0.2 mg ml^{-1}) and (b) ethanol (0.1, 0.2, 0.3 and 0.4 mg ml^{-1}), dispersed using probe-ultrasonication and (c) ethanol (1 mg ml^{-1}), dispersed using magnetic stirrer.

have lesser hole injection barrier than methanol. Therefore, charge transfer nature will be changed for different solvents. HOMO and LUMO of adsorbates i.e. OA and TOP are not considered for simplicity, they however will also involve in this charge transfer mechanism. Hence, the combination of all means metal/surfactant and solvent give such type of features, which is difficult to rule out here [45]. P2 is split or oscillate in methanol, ethanol, DIW and n-hexane in three, four, five and seven, respectively. The number of split peaks is different in these solvents, which may be understood through their different charge-transfer nature, electronegativity, chain length and coverage of molecules, and hence surface charge density or interface dipole [42]. Considering their dipole moment strengths as 1.7, 1.7, 1.87 and 0.08 D, respectively [46–48], however, while there appears to have no direct correlation on number of peaks split on SPR response, there exists significant influence on it individually.

The transferred charge or formed dipoles may oscillate with slightly different frequency than that in air, which leads to splitting in SPR. Furthermore, the higher ζ is related to larger surface charge density or more dipoles, which may result in more oscillations in P2 in n-hexane than other solvents [42]. In addition, larger blue-shift in P2 in n-hexane compared to ethanol is observed while they have nearly equal value of μ, which is due to availability of different number of electrons [36]. Less ζ and larger HD in ethanol compared to n-hexane indicates more agglomeration of NPs or decrease in interparticle distance, which is consistent with FESEM micrographs (figure 8). As a consequence, red-shift and new peak may appear in optical spectra compared to a single or unagglomerated NP, due to coupling of plasmon modes in adjacent NPs [37]. The larger broadening, damping and asymmetry in ethanol support this picture [14].

The variation in position of SPR with μ may be explained within the framework of the Drude model. According to this model, the relation between peak position of SPR (λ) and optical dielectric function of the medium (ε_m) can be written as [49]

$$\lambda^2 = \lambda_P^2(\varepsilon^\alpha + 2\varepsilon_m),$$

where λ_P and ε^α are the bulk metal plasmon wavelength and high frequency dielectric constant due to inter-band and core transitions, respectively. Therefore, the graph between $\lambda^2/1000$ versus $2\varepsilon_m$ are plotted (figure 17). Non-linearity is seen in polar solvents but straight line in non-polar solvents, which indicates that μ affects the position of SPR in the frame-work of Drude model only in nonpolar solvents, not in polar solvents [49]. Therefore, it is inferred that SPR is highly sensitive to μ and polarity that shows the extended features.

Further, to check our hypothesis of peak splitting, we performed UV–Visible measurements with varying concentration of NPs, ultrasonication time and amplitude in ethanol and n-hexane. UV–Visible spectra of Ag4 were recorded by varying the concentration of NPs using their dilution followed by probe-ultrasonication (of frequency 20 KHz) for 5 min in each time (figure 18). As concentration of NPs increases, SPR gets narrower with enhanced absorbance and gradually blue-shifted. Five (two) peaks can be clearly seen, while two (one)

peaks are feeble in ethanol (n-hexane) for 5 min ultrasonication. These feeble intensity peaks increase with increase in concentration and time of ultrasonication (figures 18(a) and (b), insets). Now, absorbance spectra of Ag4 in ethanol were taken for 2 min and 80% less amplitude. A hump like feature (P2) without any splitting is found, which is red-shifted. Lesser amplitude and time of ultrasonication may lead to reduced dispersity of NPs, decrease interparticle-distance, weaken the bonding between NPs and solvents molecules, and hence charge transfer effects. Therefore, we observed the tunable features of SPR in Ag NPs in broad range of ultraviolet (UV) regime, which indicates their many potential applications such as photocatalyst, UV-detector and plasmonic sensor [39, 50, 51].

Conclusion

The SPR of Ag NPs are found to be sensitive to particle size, dielectric environment and solvent refractive index. The main SPR feature shifts towards higher wavelength side (red shift), as particle size decreases or adsorbate coverage increases. The solvent refractive (μ) of methanol, deionized water, ethanol, n-hexane, benzene and toluene has been used to vary μ. The main SPR feature is shifted towards higher wavelength side (red-shift) as μ increases in polar as well as non-polar solvents. We found that SPR near 320 nm in smaller NPs in air shifts to around 259 nm, 261 nm, 277 nm, 255 nm, 275 nm and 282 nm in methanol, deionized water, ethanol, n-hexane, benzene and toluene, respectively. Furthermore, the agglomeration condition studies of the NPs in these solvents using DLS through zeta-potential (ζ), HD, mobility and conductivity for their correlation with SPR well-support the interactions that are taking place among the NPs and solvents. This has further been substantiated using a model for re-adjustment of the Fermi level of Ag NP and HOMO and LUMO of surface-bound solvents. Finally, the multiple peak features of SPR in ultraviolet region indicate their potential applications such as photocatalyst, UV-sensor and detector.

Acknowledgments

Authors would like to acknowledge Dr D M Phase/Mr Gyanendra Panchal Mr V Ahire, Dr R J Choudhary and Dr U Deshpande/Mr Prakash Behera, UGC-DAE Consortium for Scientific Research, Indore, India for providing XRD/EDX, XPS and FTIR and UV–Visible reflectance data, respectively. Authors are thankful to USIF, Aligarh Muslim University, Aligarh and CIL, Dr Harisingh Gour University, Sagar and Dr Subha Jain, Vikram University, Ujjain, India for providing HRTEM, FESEM and UV–Visible absorbance data, respectively. UGC-DAE Consortium for Scientific Research, Indore funded this research as a routine work.

ORCID iDs

Vikash Sharma https://orcid.org/0000-0002-9277-4411
Divya Verma https://orcid.org/0000-0003-4802-6368
Gunadhor Singh Okram https://orcid.org/0000-0002-0060-8556

References

[1] Peng S, McMahon J M, Schatz G C, Gray S K and Sun Y 2010 *Proc. Natl Acad. Sci.* **107** 14530
[2] Barnes W L, Dereux A and Ebbesen T W 2003 *Nature* **424** 824
[3] Alshehri A H, Jakubowska M, Młożniak A, Horaczek M, Rudka D, Free C and Carey J D 2012 *ACS Appl. Mater. Interfaces* **4** 7007
[4] Gong J, Dai R, Wang Z and Zhang Z 2015 *Sci. Rep.* **5** 1
[5] Sun Y, Gates B, Mayers B and Xia Y 2002 *Nano Lett.* **2** 165
[6] Barakat N A M, Woo K Do, Kanjwal M A, Choi K E, Khil M S and Kim H Y 2008 S *Langmuir* **24** 11982
[7] Sheldon M T, van de Groep J, Brown A M, Polman A and Atwater Harry A 2014 *Science* **346** 828
[8] Shen W, Zhang X, Huang Q, Xu Q and Song W 2014 *Nanoscale* **6** 1622
[9] Tran Q H, Nguyen V Q and Le A T 2013 *Adv. Nat. Sci.* **4** 033001
[10] Sharma V K, Yngard R A and Lin Y 2009 *Adv. Colloid Interface Sci.* **145** 83–96
[11] Frazer R A 2011 *J. Nanomed. Nanotechnol.* **03** 1
[12] Chernousova S and Epple M 2013 *Angew. Chem., Int. Ed. Engl.* **52** 1636
[13] Kelly K L, Coronado E, Zhao L L and Schatz G C 2003 *J. Phys. Chem.* B **107** 668
[14] Amendola V, Bakr O M and Stellacci F 2010 *Plasmonics* **5** 85
[15] Mahmoud M A, Chamanzar M, Adibi A and El-Sayed M A 2012 *J. Am. Chem. Soc.* **134** 6434
[16] Sharma V, Chotia C, Tarachand T, Ganesan V and Okram G S 2017 *Phys. Chem. Chem. Phys.* **19** 14096
[17] Scholl J A, Koh A L and Dionne J A 2012 *Nature* **483** 421
[18] Liu X, Li D, Sun X, Li Z, Song H, Jiang H and Chen Y 2015 *Sci. Rep.* **5** 1
[19] Wiley B J, Im S H, Li Z Y, McLellan J, Siekkinen A and Xia Y 2006 *J. Phys. Chem.* B **110** 15666
[20] Mogensen K B and Kneipp K 2014 *J. Phys. Chem.* C **118** 28075
[21] Yoon J W, Koh G M, Song S H and Magnusson R 2012 *Phys. Rev. Lett.* **109** 2
[22] Wang Y, Zheng Y, Huang C Z and Xia Y 2013 *J. Am. Chem. Soc.* **135** 1941
[23] Hutter E and Fendler J H 2004 *Adv. Mater.* **16** 1685
[24] Yu Y, Jiang Y, Tang Z, Guo Q, Jia J, Xue Q, Wu K and Wang E 2005 *Phys. Rev.* B **72** 205405
[25] Lee E J, Kim Y H, Hwang D K, Choi W K and Kim J Y 2016 *RSC Adv.* **6** 11702
[26] Jang H W, Kim Y H, Lee K W, Kim Y M and Kim J Y 2017 *APL Mater.* **5** 080701
[27] Okram G S, Devi K N, Sanatombi H, Soni A, Ganesan V and Phase D M 2008 *J. Nanosci. Nanotechnol.* **8** 4127
[28] El Mel A A, Stephant N, Hamon J, Thiry D, Chauvin A, Chettab M, Gautron E, Konstantinidis S, Granier A and Tessier P Y 2016 *Nanoscale* **8** 141
[29] Singh J, Kaurav N, Lalla N P and Okram G S 2014 *J. Mater. Chem.* C **2** 8918
[30] Mourdikoudis S and Liz-marza L M 2013 *Chem. Mater.* **259** 1465
[31] Togashi T, Nakayama M, Hashimoto A, Ishizaki M, Kanaizuka K and Kurihara M 2018 *Dalton Trans.* **47** 5342
[32] Chen S, Zhang X, Zhang Q and Tan W 2009 *Nanoscale Res. Lett.* **4** 1159
[33] Zhang Z, Zhang X, Xin Z, Deng M, Wen Y and Song Y 2011 *Nanotechnology* **22** 425601

[34] Koczkur K M, Mourdikoudis S, Polavarapu L and Skrabalak S E 2015 *Dalton Trans.* **44** 17883
[35] Delgado A V, González-Caballero F, Hunter R J, Koopal L K and Lyklema J 2007 *J. Colloid Interface Sci.* **309** 194
[36] Sun D, Kang S, Liu C, Lu Q, Cui L and Hu B 2016 *Int. J. Electrochem. Sci.* **11** 8520
[37] Halas N J, Lal S, Chang W-S, Link S and Nordlander P 2011 *Chem. Rev.* **111** 3913
[38] Huang K, Pan W, Zhu J F, Li J C, Gao N, Liu C, Ji L, Yu E T and Kang J Y 2015 *Sci. Rep.* **5** 1
[39] Knight M W, King N S, Liu L, Everitt H O, Nordlander P and Halas N J 2014 *ACS Nano* **8** 834
[40] Arumugam D, Thangapandian M, Jayaram A, Okram G S, Lalla N P, Franklin M and Amirtham B 2016 *J. Phys. Chem.* C **120** 26544
[41] Koch N, Kahn A, Ghijsen J, Pireaux J J, Schwartz J, Johnson R L and Elschner A 2003 *Appl. Phys. Lett.* **82** 70
[42] Goldys E M and Sobhan M A 2012 *Adv. Funct. Mater.* **22** 1906
[43] Hayakawa T, Nagai M, Yamamoto M, Makimura M and Nemoto K 2004 *Int J Oral- Med Sci.* **3** 20
[44] Sreekala C O, Jinchu I, Sreelatha K S, Janu Y, Prasad N and Kumar M 2012 *IEEE J. Photovolt.* **2** 312
[45] Han P, He Y, Chen C, Yu H, Liu F, Yang H, Ma Y and Zheng Y 2016 *Sci. Rep.* **6** 1
[46] http://murov.info/orgsolvents.htm
[47] www.chemistry.mcmaster.ca/adronov/resources/Common_Solvents_for_Organic_Reactions.pdf
[48] https://people.chem.umass.edu/xray/solvent.html
[49] Nath S, Ghosh S K, Praharaj S, Panigrahi S, Basu S and Pal T 2005 *New J. Chem.* **29** 1527
[50] Eom H, Jung J Y, Shin Y, Kim S, Choi J H, Lee E, Jeong J H and Park I 2014 *Nanoscale* **6** 226
[51] Okamoto K and Tamada K 2014 *ACS Symp. Ser.* **1246** 247